ACS OMEGA

http://pubs.acs.org/journal/acsodf

Article

Raman Spectroscopy Characterization of Amorphous Coke Generated in Industrial Processes

Claire Chunjuan Zhang, Sage Hartlaub, Ivan Petrovic, and Bilge Yilmaz*

Cite This: *ACS Omega* 2022, 7, 2565−2570

Read Online

ACCESS | Metrics & More | Article Recommendations | Supporting Information

ABSTRACT: Examples on the real-world field application of Raman spectroscopy with systematic analysis of the intensity variation of D and G bands corresponding to the change of excitation laser energy to characterize and compare coke species from various industrial processes are presented. The findings indicate the different degree of sp^2 and sp^3 hybridized bonding structures of amorphous carbon collected from different industrial processes as well as heavy carbonaceous deposits generated by industrial catalysts. This spectroscopic methodology is practical and highly beneficial in identifying coke formation mechanisms in industrial processes, as well as supporting design strategies to abate the undesired coke formation on industrial catalysts.

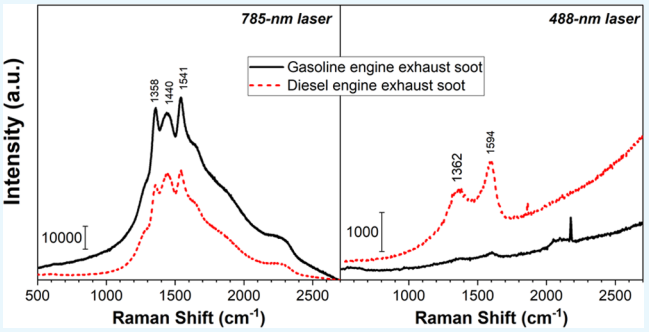

1. INTRODUCTION

As part of the standardized industrial chemical terminology, coke is defined as the carbonization product of high-boiling hydrocarbon fractions obtained in petroleum processing.[1] Coke is typically formed in many industrial processes, such as thermolysis of petroleum residues, crude oil transportation in pipeline networks, catalytic refining processes such as fluid catalytic cracking (FCC), and the combustion of their product fuels (e.g., gasoline and diesel) in internal combustion engines.[2,3] For efficacy and durability of many industrial catalysts, coke formation/deposition and removal are defining factors. Therefore, there is a desire to develop a better understanding of coke as well as its formation and subsequent transformations in various industrial processes. Different coke formation mechanisms impact the coke crystalline structure (e.g., sp^2 and sp^3 hybridized bonding). The coke formed in the processes mentioned above is usually amorphous with a mixture of sp^2, sp^3, and even sp^1-bonded sites. Depending on the ratio of these sites, amorphous carbons often show different optical, electrical, and mechanical properties. Undesired coke can be removed via various processes including combustion and gasification. Coke with different crystalline structures also presents varying physical properties and activities in the gasification process. Determining the coke long-range crystalline and short-range bonding structure can help with the identification of coke formation mechanisms, as well as the design of effective strategies for coke removal.

Raman spectroscopy measures the counts of photons that are scattered from a sample surface when an excitation laser shines on the sample. During the scattering process, the excitation photons interact with the molecular bond vibrations leading to the energy shift of the scattered photons. This energy shift is called the Raman shift, which is a specific characteristic of the bond vibration and can be used as the "fingerprint" of underlying materials and structures. Raman spectroscopy is a particularly well-suited technique to characterize carbon crystallinity.[4−9] The long-range crystalline vibrations and short-range molecular vibrations of carbon species in different materials result in characteristic fingerprints in Raman shifts that can help identify specific carbon materials including graphite, diamond, graphene, carbon nanotubes, fullerene, and amorphous carbon. A diamond sample has a Raman response at 1332 cm^{-1}, and a crystalline graphite sample has Raman responses at 1582 (G, a primary in-plane mode) and 2700 cm^{-1} (G′ or 2D, a secondary overtone of an in-plane mode). Detailed investigations on various graphene samples are also reported in the literature.[10,11] Recently, there have also been significant advances in theoretical and computational studies exploring graphene, bilayer graphene, and two-dimensional graphene heterostructures.[12,13]

An amorphous carbon sample has Raman responses at 1355 (D) and 1575 (G) cm^{-1}, where G bands represent the graphite-type lattice vibrations with E_{2g} symmetry and D bands reflect the disordered graphite lattice vibrations with A_{1g} symmetry.[14−19] A comprehensive theoretical study of Raman spectra in disordered and amorphous carbon from Ferrari and

Received: July 1, 2021
Accepted: November 22, 2021
Published: January 3, 2022

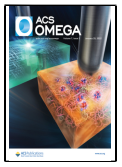

https://doi.org/10.1021/acsomega.1c03456
ACS Omega 2022, 7, 2565−2570

Robertson provided a three-stage model that shows the variation of G band positions and the intensity ratios of D and G bands (I_D/I_G) as the amorphization trajectory changes.[4,15] The spectral analysis from Pöschl et al. provided a detailed Raman peak deconvolution of the D_1, D_2, D_3, D_4, and G bands under multiple excitation laser energies for soot materials, where D_1, D_2, and D_4 bands with a Lorentzian line shape refer to the disordered graphitic lattice of different symmetries, D_3 refers to amorphous carbon with a Gaussian line shape, and G bands refer to the in-plane graphitic lattice of E_{2g} symmetry with a Lorentzian line shape.[17] In recent years, pyrolysis is gaining significant attention with increased emphasis on sustainability, where the nature and transformation of amorphous carbonaceous species are also studied in detail with the help of Raman spectroscopy.[20,21]

In this contribution, multiple examples are studied using Ferrari and Pöschl's models to qualitatively identify the degree of sp^2 and sp^3 hybridized bonding structures using Raman spectroscopy in amorphous coke collected in thermolysis of petroleum residues, crude oil transportation in pipeline networks, gasoline/diesel combustion engines, and filtered slurry collected from the fluid catalytic cracking (FCC) process. As described in the literature, the change in excitation laser energy can be a prolific approach to derive bonding structure information.[18] The main focus of this investigation is the application of two different lasers with visible excitation energies on coke samples generated in various industrial processes, which could serve as a practical and convenient method to get bonding structure information on coke samples.

2. RESULTS AND DISCUSSION

2.1. Operando Raman Spectroscopy. One of the carbon removal processes is the gasification process, which converts unwanted coke materials to carbon dioxide through catalytic reactions.[22] To study the coke transformations via the gasification process, mixtures of different coke samples were prepared and heat-treated together with manganese oxide under a steam−argon atmosphere for the gasification process.

Manganese oxide is a mixed-oxidation-state material, which is widely used in the gasification process to provide the source of active oxygen.[23,24] As shown in Figure S1 as part of the Supporting Information, oxygen can be generated upon heating the powder of Mn_2O_3 in a 0.5% steam−Ar environment due to self-decomposition of Mn_2O_3. A further study on the mixture of Mn_2O_3 and 10% carbon shows three regions (#1: 600−770 °C; #2: 770−850 °C; #3: 850 °C or a longer time at ≥800 °C) for gasification based on the gaseous products as shown in Figure S2. The gasification processes involve a self-reduction of manganese oxide, oxidation of coke, and water-gas shift reactions. The proposed reactions are given in the Supporting Information, which is not the essential objective of this manuscript. In order to get a clear picture of the change of the solid structure of manganese oxide during the gasification process, a mixture of Mn_3O_4 and 10% carbon was heated in Argon up to 850 °C. This process was monitored by the operando Raman method, coupling Raman and mass spectroscopy (MS) for gas products and the solid surface structure change under reaction conditions. Figure 1 shows the Raman spectra (using a 785 nm laser) on the solid surface collected at 30 (before gasification) and 850 °C (under gasification). It should be noted that the second spectrum was collected for a temperature window of 770−850 °C so that the surface state of manganese oxide can be captured in the regions

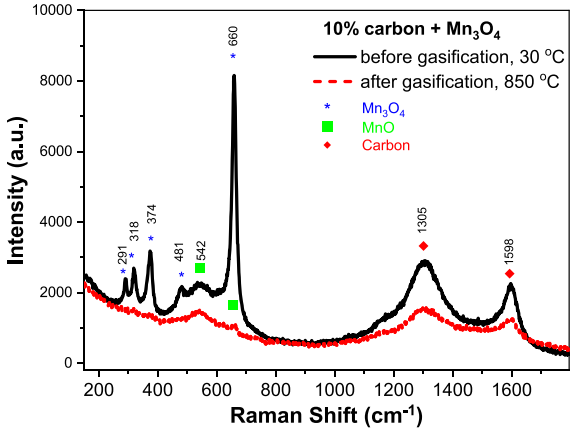

Figure 1. Raman spectra under a 785 nm laser with 10% power, 2 scans at 60 s per scan before and after gasification for 10% carbon (Sample #1) mixed with Mn_3O_4 powder. The peak assignments are marked by blue stars (*) for Mn_3O_4, green squares for MnO, and red diamonds for amorphous carbon.

#1 and #2 (as mentioned above) before the evolution of a large amount of H_2 due to water-gas shift reactions. As shown in Figure 1, before the gasification process started, the Raman spectrum shows the Mn_3O_4 phase with signals at 291, 318, 374, 481, and 660 cm^{-1}.[22] As the gasification process has been completed at 850 °C, the Raman spectrum shows the MnO phase at 542 and 660 cm^{-1}.[25] The Raman spectra show that the solid surface changes from Mn_3O_4 to MnO, and the amount of carbon is reduced after gasification. Although the detailed reaction mechanism is complicated as discussed earlier, a simplified net gasification reaction is given below

$$C + 2Mn_3O_4 \rightarrow 6MnO + CO_2 \quad (1)$$

Interestingly, the CO_2 release activity is significantly different for a second coke sample, which was obtained from the deposits formed in a crude oil transportation pipeline, as shown in the MS data in Figure 2. The CO_2 released from coke Sample #1 gasification is higher than that from coke Sample

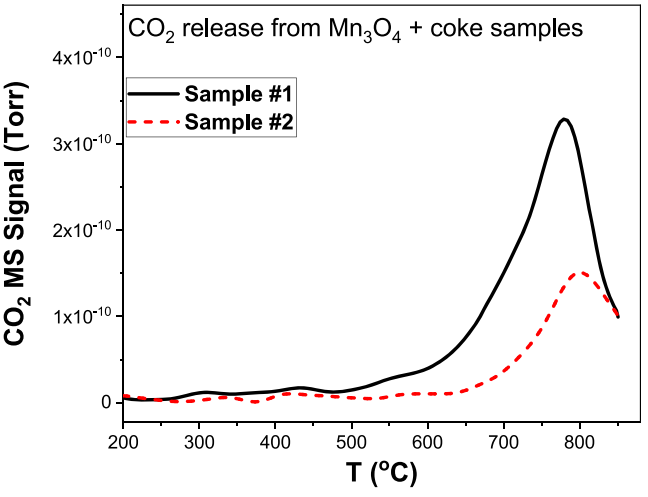

Figure 2. Mass spectra of temperature-dependent CO_2 gasification for two different types of carbons (Samples #1 and #2) mixed with Mn_3O_4 powder. Experiments were conducted with a temperature ramp rate of 10 °C/min, using Ar as a carrier gas with a flow rate of 100 mL/min.

https://doi.org/10.1021/acsomega.1c03456
ACS Omega 2022, 7, 2565−2570

#2, and the onset temperature is about 50 °C lower than that of coke Sample #2. This result indicates the retardation of the gasification reaction for coke Sample #2 (i.e., delay of the gasification reaction).

The activity difference of the two types of coke can be explained by the bonding variation observed in the operando Raman spectra during the gasification processes. Figure 3

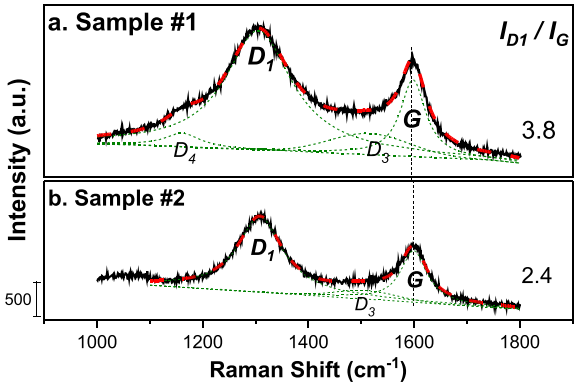

Figure 3. (a,b) Peak fittings for Raman spectra of the two types of coke under a 785 nm laser with 10% power, 2 scans at 60 s per scan. The background was chosen as a linear background. $I(D_1)/I(G)$ ratios for coke Samples #1 and #2 are 3.8 and 2.4, respectively. The G peak positions are at 1598 and 1599 cm^{-1} for Samples #1 and #2, respectively.

shows the peak fittings of the D and G peaks in the Raman spectra. The peak deconvolution was conducted using the three-stage model reported by Ferrari and Robertson.[4,15] and the five-peak model reported by Pöschl et al.[17] The deconvoluted peaks include the Lorentzian shape and the Gaussian shape for phonon finite lifetime broadening and random lifetime broadening, respectively. The G peak represents ideal graphitic vibrations with E_{2g} symmetry, which can be found in graphitic rings and chains consisting of sp^2 C atoms.[4] The D peaks represent the breathing mode of the six-member ring of carbon or disordered graphitic vibrations with A_{1g} symmetry at ~1305 (D_1 band with a Lorentzian shape) and ~1160 cm^{-1} (D_4 band with a Lorentzian shape), with Gaussian-type D_3 at ~1510 cm^{-1}, and with E_{2g} symmetry at ~1650 cm^{-1} (D_2 band with a Lorentzian shape).[17] The sp^2 and sp^3 content in the amorphous carbon depends on the ratio of $I(D_1)/I(G)$ and the position of the D and G peaks.[4] Based on the peak fitting data shown in Figure 3 and Table 1, $I(D_1)/I(G)$ ratios for the coke Samples #1 and #2 are 3.8 and 2.4, respectively. The standard errors of Monte Carlo calculations for the fitting are given for the confidence levels of the fitting results. The G peak positions are at 1598 and 1599 cm^{-1} for coke Samples #1 and #2, respectively. Both coke Samples #1 and #2 have structural spectroscopic responses close to nanocrystalline graphite.[4] The comparison of $I(D_1)/I(G)$ ratios for the two samples indicates the higher degree of graphitization for coke Sample #1. On the other hand, the chemical activity data (Figure 2) also show coke Sample #1 as having a higher activity in the reaction with Mn_3O_4. This example shows a correlation of coke activity with its structure, which suggests the importance of an in-depth understanding of the carbon structural properties for a better understanding of its activity performance.

One reason for seeing lower overall carbon signals in Figure 3 when using a 785 nm Raman laser can be due to the different amount of coke in the detecting area on the mixture sample. There is also another possibility due to the different degree of structural disorder—the different ratio of sp^2 and sp^3 bonding. To further investigate the different ratio of sp^2 and sp^3 bonding, ex situ Raman analysis was performed on the second set of samples, which come from the soot of gasoline (Sample #3) and diesel (Sample #4) engines.

2.2. Ex Situ Raman Spectroscopy. Visible Raman spectroscopy is more sensitive to π-bond (sp^2) than σ-bond (sp^3) vibrations due to the fact that π bonds are more polarizable (a larger Raman cross section) than σ bonds.[4,15,17,18] Increasing the excitation laser energy can increase the detecting cross section, which makes the σ-bond (sp^3) vibrations more sensible.[17,18] Therefore, in this Raman analysis, two laser energies were used to identify the carbon long-range crystallinity and short-range bonding disorders of the samples. The 785 nm laser excitation (shown in Figure 4a) is more sensitive to the π-bond (sp^2) vibrations, and the 488 nm laser (shown in Figure 4b) is more sensitive to the σ-bond (sp^3) vibrations. The gasoline soot (Sample #3) shows a higher intensity for amorphous carbon peaks than the diesel soot with the 785 nm excitation laser energy (the black trace on top of the red trace), and a reversed intensity order is observed for the 488 nm laser (the red trace on top of the black trace). For each sample, the Raman spectrum was collected under the 785 nm laser; then, another spot on the same sample was chosen when switching to the 488 nm laser to minimize the possibility of any change associated with excitation lasers. The alternated order of peak intensities in Raman spectra under the two lasers suggests a change of Raman signal sensitivity in this region correlated with excitation energy. The π bond (sp^2) is more impacted by the change of excitation energy due to its

Table 1. Raman Peak Deconvolution Results for Spectra in Figure 3

laser	center (cm^{-1})	peak type	area integrated, relative (%)	area integrated, standard error (yEr±, %)	FWHM	peak assignment	I_{D1}/I_G
Sample #1, 785 nm	1162	Lorentzian	4.2	0.3	82	D_4	
	1306	Lorentzian	66.1	1.0	152	D_1	3.8
	1515	Gaussian	10.8	4.3	179	D_3	
	1598	Lorentzian	17.5	0.8	58	G	
	1650	Lorentzian	1.4	6.1	300	D_2	
Sample #2, 785 nm	1158	Lorentzian	0.0	0.0	5	D_4	
	1308	Lorentzian	64.6	1.2	102	D_1	2.4
	1510	Gaussian	7.4	3.4	138	D_3	
	1599	Lorentzian	26.9	1.5	60	G	
	1650	Lorentzian	1.0	7.3	300	D_2	

https://doi.org/10.1021/acsomega.1c03456
ACS Omega 2022, 7, 2565−2570

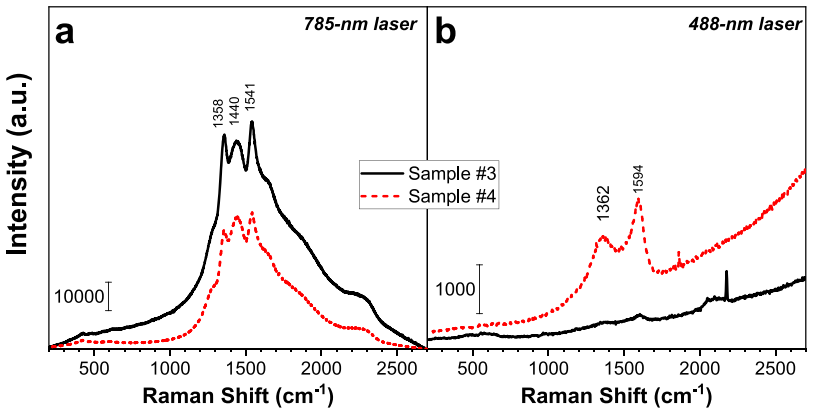

Figure 4. Raman spectra of gasoline and diesel soot powders (Samples #3 and #4) with (a) 785 nm laser with 0.1% power, 2 scans at 60 s per scan, and (b) 488 nm excitation laser with 100% power, 2 scans at 60 s per scan.

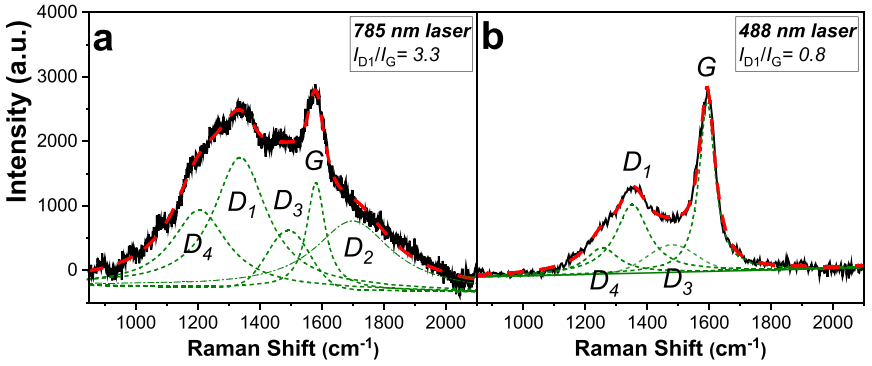

Figure 5. Raman spectra (deconvoluted in green) of a filtered slurry sample from FCC processes (Sample #5) under (a) 785 nm with 10% power, 2 scans at 60 s per scan, and (b) 488 nm excitation lasers with 100% power, 2 scans at 60 s per scan.

Table 2. Raman Peak Deconvolution Results for Spectra in Figure 5

laser	center (cm^{-1})	peak type	area integrated, relative (%)	area integrated, standard error (yEr±, %)	FWHM	peak assignment	I_{D1}/I_G
785 nm	1205	Lorentzian	21.1	4.1	216	D_4	
	1337	Lorentzian	34.8	7.3	208	D_1	3.3
	1492	Gaussian	9.0	3.3	160	D_3	
	1581	Lorentzian	10.5	1.8	72	G	
	1700	Lorentzian	24.6	1.2	300	D_2	
488 nm	1255	Lorentzian	12.6	4.1	127	D_4	
	1352	Lorentzian	33.1	8.9	128	D_1	0.8
	1479	Gaussian	13.8	5.6	185	D_3	
	1594	Lorentzian	40.5	2.2	62	G	
	1735	Lorentzian	0.0	0.0	5	D_2	

resonance effect in the visible wavelength range. At a qualitative level, this result suggests that the gasoline soot has more sp^2 content, and the diesel soot (Sample #4) has more sp^3 content. Both samples are amorphous carbon with graphite-like local crystallinity. A fine-size effect can be seen by the broadening of the peaks. Defect sites on the graphite-like sheets exist with evidence of a pentagonal pinch vibration mode at 1440 cm^{-1}.

Further analysis of a third type of hydrocarbon sample (Sample #5) is shown in Figure 5 and Table 2. This sample is filtered carbonaceous powder from the slurry generated by an actual fluid catalytic cracking (FCC) unit that is processing a heavy-resid feedstock. Under the two excitation laser energies (785 and 488 nm), the Raman spectra show significantly decreased $I(D_1)/I(G)$ ratio (from 3.3 to 0.8) and an upper shift of the G position (1581 to 1594 cm^{-1}). As pointed out by Ferrari and Robertson, the decrease in the $I(D_1)/I(G)$ ratio and the upper shift of the G peak position indicate the greater impact from sp^3 for chain-type structures.[4] This example clearly demonstrates that by changing the excitation laser energy from 785 to 488 nm, sp^3 hybridized bond features are more sensible in Raman spectroscopy.

As seen in the experimental results presented above, systematic analysis of the intensity variation of D and G bands corresponding to the change of excitation laser energy indicates significant diversity with varying degrees of sp^2 and sp^3 hybridized bonding structures for coke species collected from different industrial processes as well as heavy carbonaceous deposits generated by industrial catalysts. Catalytic formation of coke can be described as transformation of carbonaceous species into structures that contain a further delocalized bond electron distribution. The varying ratios of

https://doi.org/10.1021/acsomega.1c03456
ACS Omega 2022, 7, 2565−2570

sp^3 to sp^2 bonding structures in these diverse sets of samples highlight the variation in the conjugated π electron system based on the nature of the process and catalysts as well as the precursors.

Other established characterization techniques such as ^{13}C solid-state nuclear magnetic resonance (ssNMR) spectroscopy have been employed for elucidation of the structure of coke-type carbonaceous species from industrially relevant processes such as biomass conversion[26] for many decades. Coupling this technique with the type of systematic Raman spectroscopy investigation presented in this contribution can further increase the insights gained into coke formation in industrial processes and into industrial catalysts in terms of the enhanced structural resolution. Recent technical advances in the field of ssNMR, such as new magic angle spinning probes, high-field spectrometers, and superior pulse sequences for spectral editing, make the combination of these techniques even more powerful in such structural analyses on industrial coke samples and mechanistic studies on coke formation in industrial processes.

There are also new characterization methods that have been developed in recent years that can provide critical information for monitoring catalyst coking and deactivation in industrial catalytic processes. A prominent example is the new microwave-based approach[27] that investigates the nature of catalytic coke formation as an evolution from sp^3 carbons to sp^2 carbons that possess a further delocalized bond electron distribution. This novel nonintrusive method is based on microwave cavity perturbation analysis for characterization of both the amount and the chemical composition of coke species formed over catalysts with sample full-body penetration.[27] In this technique, the obtained dielectric loss value reflects the overall coke amount, and different compositions of coke lead to markedly different absorption efficiencies. This new and practical technique can also be effectively used in combination with the systematic Raman spectroscopy approach highlighted in this contribution to complement and further validate the results generated by Raman spectroscopy.

3. MATERIALS AND METHODS

For sample information, detailed descriptions are listed in Table 3. Samples #1−5 were investigated by operando Raman spectroscopy for coke characterization. Samples #1 and #2 were two types of coke collected in two industrial processes—thermolysis of petroleum residues and crude oil transportation in pipeline networks. These two coke materials were mixed with manganese oxide (Mn_3O_4) (Sigma Aldrich) and analyzed by operando Raman spectroscopy during high-temperature gasification processes. Samples #3 and #4 were two soot carbon materials collected at the gasoline/diesel engine exhaust. The mixtures of coke and manganese oxide were ground into fine powders with a mortar and pestle.

Table 3. Powder Sample IDs and Description

sample ID	description
1	coke from thermolysis of petroleum residues
2	coke deposited during crude oil transportation in pipeline networks
3	gasoline engine exhaust soot
4	diesel engine exhaust soot
5	filtered FCC slurry from a resid-FCC unit

Raman spectra were collected on a Renishaw inVia Raman microscope with 785 and 488 nm lasers as the excitation source. A Leica N PLAN microscope/50× objective lens was used to focus the 785 nm laser beam on the sample surface at 0.1 to 10% in power usage (100% power for the 488 nm laser). The ground powder samples were loaded as a flat thin layer on a piece of a glass slide. Raman spectra were collected repeatedly under the same excitation laser after changing to the other laser in order to check for possible beam damage. There was no significant change in the Raman signals after the switch, which suggests that there was no detectable beam damage in these experiments.

Operando Raman analysis was conducted on the mixture of 10% carbon with manganese oxide (Mn_3O_4) powder. The ground powder mixture (~40 mg) was loaded into a Linkam CCR 1000 reactor and heated up to 850 °C at a ramping rate of 10 °C/min under a steam−Ar environment, maintained at 850 °C for 10 min, and cooled down (20 °C/min) under the same environment to 30 °C. A mass spectrometer (Hiden Analytical, Inc., HPR2030) was used to monitor the formation of H_2O, H_2, O_2, CO, and CO_2 as a function of temperature. Raman spectra were also collected before and after treatment.

4. CONCLUSIONS

Industrial examples are provided on the use of operando Raman spectroscopy for characterization of crystalline structures and bonding configurations of carbonaceous samples obtained at various stages of petroleum processing and utilization. Gasification activities of coke from different sources were studied in detail by comparing the $I(D_1)/I(G)$ ratio and the G peak position. To explore the ratio of sp^2 and sp^3 bonding in greater detail, an ex situ Raman analysis was conducted using two lasers with different excitation energies on the filtered slurry samples from the fluid catalytic cracking process as well as soot powders from gasoline and diesel engines. By changing the excitation energy of the laser, the sensitivity of Raman signals was modified for the π bond (sp^2) and σ bond (sp^3) vibrations. With this approach, the gasoline soot was found to have more sp^2 content, and the diesel soot has more sp^3 content. This methodology proves to be a practical means to support research activities by identifying coke structural variation in various industrial processes and its correlation with activities, which could help efforts on developing methods for targeted coke removal for different crystalline structures. For further insights into the nature of coke formation in industrial processes and into industrial catalysts, solid-state ^{13}C NMR spectroscopy[22] and dielectric measurements via microwave cavity perturbation analysis[23] can be utilized to complement the results generated by Raman spectroscopy.

■ ASSOCIATED CONTENT

Supporting Information

The Supporting Information is available free of charge at https://pubs.acs.org/doi/10.1021/acsomega.1c03456.

(Figure S1) Mass spectrum of oxygen (mass of 32) evolution during the heating process of Mn_2O_3 powder in a 0.5% steam−argon atmosphere; (Figure S2) mass spectra of CO_2 (mass of 44), CO (mass of 28), and H_2 (mass of 2) evolution during the heating process of a

https://doi.org/10.1021/acsomega.1c03456
ACS Omega 2022, 7, 2565−2570

10% C and Mn_2O_3 mixture in 0.5% steamed argon (PDF)

AUTHOR INFORMATION

Corresponding Author

Bilge Yilmaz − *BASF Corporation, Iselin, New Jersey 08830, United States;* orcid.org/0000-0001-9083-4065; Email: bilge.yilmaz@basf.com

Authors

Claire Chunjuan Zhang − *BASF Corporation, Iselin, New Jersey 08830, United States;* orcid.org/0000-0002-9402-4702

Sage Hartlaub − *BASF Corporation, Iselin, New Jersey 08830, United States*

Ivan Petrovic − *BASF Corporation, Iselin, New Jersey 08830, United States*

Complete contact information is available at: https://pubs.acs.org/10.1021/acsomega.1c03456

Author Contributions

C.C.Z. and B.Y. performed the conceptualization and investigation; C.C.Z. performed the methodology, formal analysis, visualization, and project administration; I.P. acquired resources; C.C.Z. and S.H. performed the data curation; C.C.Z. and B.Y. wrote the original draft; C.C.Z., S.H., B.Y., and I.P. reviewed and edited the manuscript; B.Y. and I.P. performed supervision; B.Y. performed funding acquisition. All authors have given approval to the final version of the manuscript.

Notes

The authors declare no competing financial interest.

ACKNOWLEDGMENTS

The authors would like to thank Jeff Hoke, Ron Russo, and Pavel Ruvinskiy for their support.

REFERENCES

(1) McNaught, A. D.; Wilkinson, A. *IUPAC Compendium of Chemical Terminology, The Gold Book*, 2nd Edition, Blackwell Science: Oxford, 1997.

(2) Wiehe, I. A. A phase-separation kinetic model for coke formation. *Ind. Eng. Chem. Res.* **1993**, *32*, 2447−2454.

(3) Clough, M.; Pope, J. C.; Lin, L. T. X.; Komvokis, V.; Pan, S. S.; Yilmaz, B. Nanoporous materials forge a path forward to enable sustainable growth: Technology advancements in fluid catalytic cracking. *Microporous Mesoporous Mater.* **2017**, *254*, 45−58.

(4) Ferrari, A. C.; Robertson, J. Interpretation of Raman spectra of disordered and amorphous carbon. *Phys. Rev. B* **2000**, *61*, 14095−14107.

(5) Boppart, H.; van Straaten, J.; Silvera, I. F. Raman spectra of diamond at high pressures. *Phys. Rev. B* **1985**, *32*, 1423−1425.

(6) Filik, J. Raman spectroscopy: a simple, non-destructive way to characterize diamond and diamond-like materials. *Spectrosc. Eur.* **2005**, *17*, 10−17.

(7) Iijima, S. Helical microtubules of graphitic carbon. *Nature* **1991**, *354*, 56−58.

(8) Wall, M. Raman spectroscopy optimizes graphene characterization. *Adv. Mater. Processes* **2012**, *170*, 35−38.

(9) Ferrari, A. C. Determination of bonding in diamond-like carbon by Raman spectroscopy. *Diamond Relat. Mater.* **2002**, *11*, 1053−1061.

(10) Cui, L.; Wang, J.; Sun, M. Graphene plasmon for optoelectronics. *Rev. Phys.* **2021**, *6*, 100054.

(11) Lin, W.; Cao, E.; Zhang, L.; Xu, X.; Song, Y.; Liang, W.; Sun, M. Electrical enhanced hot holes driven oxidation catalysis at the interface of plasmon-exciton hybrid. *Nanoscale* **2018**, *10*, 5482.

(12) Mu, X.; Sun, M. The linear and non-linear optical absorption and asymmetrical electromagnetic interaction in chiral twisted bilayer graphene with hybrid edges. *Materials Today Physics* **2020**, *14*, 100222.

(13) Cui, L.; Sun, M. Graphene Plasmon-Enhanced Polarization-Dependent Interfacial Charge Transfer Excitons in 2D Graphene-Black Phosphorus Heterostructures in NIR and MIR Regions. *J. Phys. Chem. C* **2021**, *125*, 22370−22378.

(14) Angus, J.; Hayman, C. C. Low-pressure, metastable growth of diamond and "diamondlike" phases. *Science* **1988**, *241*, 913−921.

(15) Ferrari, A. C. Raman spectroscopy of graphene and graphite: Disorder, electron-phonon coupling, doping and nonadiabatic effects. *Solid State Commun.* **2007**, *143*, 47−57.

(16) Kroto, H. W.; Heath, J. R.; O'Brien, S.; Curl, R. F.; Smalley, R. E. C60: Buckminsterfullerene. *Nature* **1985**, *318*, 162−163.

(17) Sadezky, A.; Muckenhuber, H.; Grothe, H.; Niessner, R.; Pöschl, U. Raman microspectroscopy of soot and related carbonaceous materials: Spectral analysis and structural information. *Carbon* **2005**, *43*, 1731−1742.

(18) Filik, J. Raman spectroscopy: a simple, non-destructive way to characterise diamond and diamond-like materials. *Spectrosc. Eur.* **2005**, *17*, 10.

(19) Bare, S. R.; Vila, F. D.; Charochak, M. E.; Prabhakar, S.; Bradley, W. J.; Jaye, C.; Fischer, D. A.; Hayashi, S. T.; Bradley, S. A.; Rehr, J. J. Characterization of Coke on a Pt-Re/γ-Al2O3 Re-Forming Catalyst: Experimental and Theoretical Study. *ACS Catal.* **2017**, *7*, 1452−1461.

(20) Marrakchi, F.; Zafar, F. F.; Wei, M.; Wang, S. Cross-linked FeCl3-activated seaweed carbon/MCM-41/alginate hydrogel composite for effective biosorption of bisphenol A plasticizer and basic dye from aqueous solution. *Bioresour. Technol.* **2021**, *331*, 125046.

(21) Yuan, C.; Abomohra, A. E.-F.; Wang, S.; Liu, Q.; Zhao, S.; Cao, B.; Hu, X.; Marrakchi, F.; He, Z.; Hua, Y. High-grade biofuel production from catalytic pyrolysis of waste clay oil using modified activated seaweed carbon-based catalyst. *J. Cleaner Prod.* **2021**, *313*, 127928.

(22) Bukhovko, M. P.; Yang, L.; Li, L.; Malek, A.; Davis, R. J.; Agrawal, P. K.; Jones, C. W. Gasification of Radical Coke with Steam and Steam-Hydrogen Mixtures over Manganese-Chromium Oxides. *Ind. Eng. Chem. Res.* **2020**, *59*, 10813−10822.

(23) Duan, L.; Wang, Z.; Hou, Y.; Wang, Z.; Gao, G.; Chen, W.; Alvarez, P. J. J. The oxidation capacity of Mn3O4 nanoparticles is significantly enhanced by anchoring them onto reduced graphene oxide to facilitate regeneration of surface-associated Mn(III). *Water Res.* **2016**, *103*, 101−108.

(24) Alonso, E.; Hutter, C.; Romero, M.; Steinfeld, A.; Gonzalez-Aguilar, J. Kinetics of Mn2O3−Mn3O4 and Mn3O4−MnO Redox Reactions Performed under Concentrated Thermal Radiative Flux. *Energy Fuels* **2013**, *27*, 4884−4890.

(25) Mjulien, C. M.; Massot, M.; Poinsignon, C. Lattice vibrations of manganese oxides: Part I. Periodic structures. *Spectrochim. Acta, Part A* **2004**, *60*, 689−700.

(26) Baccile, N.; Falco, C.; Titirici, M.-M. Characterization of biomass and its derived char using 13C-solid state nuclear magnetic resonance. *Green Chem.* **2014**, *16*, 4839−4869.

(27) Liu, B.; Slocombe, D. R.; Wang, J.; Aldawsari, A.; Gonzalez-Cortes, S.; Arden, J.; Kuznetsov, V. L.; AlMegren, H.; AlKinany, M.; Xiao, T.; Edwards, P. P. Microwaves effectively examine the extent and type of coking over acid zeolite catalysts. *Nat. Commun.* **2017**, *8*, 514.

NOTE ADDED AFTER ASAP PUBLICATION

This paper was published ASAP on January 3, 2022, with errors in reaction 1 due to production error. The corrected version was reposted on January 7, 2022.